Journal of Catalysis 282 (2011) 83–93

Contents lists available at ScienceDirect

Journal of Catalysis

journal homepage: www.elsevier.com/locate/jcat

Reactivity and in situ X-ray absorption spectroscopy of Rb-promoted Mo_2C/MgO catalysts for higher alcohol synthesis

Heng Shou, Robert J. Davis *

Department of Chemical Engineering, University of Virginia, 102 Engineer's Way, P.O. Box 400741, Charlottesville, VA 22904-4741, USA

ARTICLE INFO

Article history:
Received 18 February 2011
Revised 23 May 2011
Accepted 31 May 2011
Available online 12 July 2011

Keywords:
CO hydrogenation
Molybdenum carbide
Higher alcohol synthesis
X-ray absorption spectroscopy

ABSTRACT

The influences of MgO support and Rb_2CO_3 promoter on the activity and selectivity of Mo_2C-based catalysts for higher alcohol synthesis from syngas were explored. The reaction was performed in a fixed-bed reactor system operating at 573 K, 30 bar, gas flow rate of 24,000 $cm^3\ g_{Mo}^{-1}\ h^{-1}$, and H_2:CO ratio of 1:1. When promoted by Rb_2CO_3, the selectivity of alcohols over 5 wt.% Mo_2C/MgO can reach 61 C% on a CO_2-free basis, with C1–C4 hydrocarbons being the main side products. Production of higher alcohols was enhanced at high promoter loading and low conversion. Characterization by X-ray absorption spectroscopy (XAS) indicated that passivated Mo_2C/MgO was more oxidized than bulk Mo_2C, but exposure to reaction conditions for 4 h partially reduced the passivated sample. Electron microscopy and XAS confirmed that Mo_2C was highly dispersed on MgO. The Rb *K* edge structure suggested that the Rb_2CO_3 promoter was structurally modified in the reaction.

1. Introduction

Synthesis gas, composed mainly of CO and H_2, can be derived from carbon sources such as coal, oil, natural gas, or biomass. Although world-scale catalytic processes have been developed to convert synthesis gas to diesel fuel or methanol, there is a growing need for its direct conversion to higher alcohols [1–3]. These higher alcohols can be used as liquid carriers of hydrogen, which can be obtained by reforming, or as fuel additives based on their mutual solubility with gasoline and diesel fuels. Higher alcohols can also be dehydrated to olefin feedstocks used to produce polymers.

Molybdenum-based solids are among the most promising catalysts for higher alcohol synthesis (HAS) because of their relatively low cost compared with Pt-group metals. Additional advantages of Mo-based catalysts for practical applications include less severe catalyst deactivation due to coke deposition (even with a syngas containing a low H_2/CO ratio of less than 2), higher selectivity to linear alcohols (especially ethanol), and low sensitivity to CO_2 in the syngas [4]. In 1980s, The Dow Chemical Company developed potassium- and cobalt-promoted molybdenum sulfide (MoS_2) catalysts for HAS [5]. The alcohol formation rate over promoted MoS_2 was reported to be 0.1–0.4 g $gcat^{-1}\ h^{-1}$ at 513–598 K and 48–207 bars, with a selectivity to mixed alcohols (on a CO_2-free basis) as high as ~85% [6–9]. However, trace amounts of hydrogen sulfide (H_2S) in the feed were needed to sustain the performance of the MoS_2 catalysts [6]. Thus, there is an incentive to explore the reactivity of nonsulfided catalysts for HAS, among which molybdenum carbide has demonstrated some promise when properly promoted.

Consistent with the landmark discovery by Levy and Boudart [10], the reactivity of transition metal carbides (TMCs) can be similar to that of expensive Pt-group metals [11–13], especially in reactions involving the transformation of C–H bonds in hydrocarbons. For example, the hydrogenation performance of TMCs is at the same level of Pt-group metals [14,15]. Park et al. also examined the effect of potassium promotion on Fischer–Tropsch synthesis over bulk molybdenum carbide (Mo_2C) catalysts. They found that unsupported molybdenum carbide produced mostly C1–C5 alkanes in CO hydrogenation at atmospheric pressure, and the promotion of the catalyst with K_2CO_3 yielded mostly C2–C5 alkenes [16]. They also found that the promotion of Mo_2C by K_2CO_3 greatly enhanced the alcohol selectivity during CO hydrogenation and they reported 50.5% alcohol selectivity at 10.3% CO conversion at high pressure [17]. The formation of alcohols from CO hydrogenation over carbide catalysts is thought to be related to the uniformity of the alkali promoter on the carbide surface [18] and to the extent of carburization [19]. Although the promotion of alcohol synthesis by the addition of alkali to Mo_2C reduces the overall activity of the catalyst, the addition of Fe, Co, and Ni can improve the activity of the promoted system [20–27].

The objective of the current study was to explore the roles of structure and reaction conditions on catalyst performance in higher alcohol synthesis. In particular, the effects of reaction temperature, pressure, and gas flow rate on the product distribution over a Rb-promoted, magnesia-supported Mo_2C catalyst were

* Corresponding author. Fax: +1 4349822658.
E-mail address: rjd4f@virginia.edu (R.J. Davis).

0021-9517/$ - see front matter © 2011 Elsevier Inc. All rights reserved.
doi:10.1016/j.jcat.2011.05.028

investigated. Magnesia was selected as a support since basic compounds are well-recognized promoters of the reaction. X-ray absorption spectroscopy at the Mo and Rb *K* edges was used to monitor the catalyst structure in situ. Catalysts were also characterized by transmission electron microscopy (TEM), elemental analysis, X-ray powder diffraction and BET surface analysis.

2. Experimental methods

2.1. Catalyst synthesis

A 5 wt.% Mo_2C/MgO sample was prepared by temperature-programmed carburization of MoO_3/MgO with a 20 vol.% CH_4/H_2 mixture. Magnesia (UBE ultrafine single crystal, >99.98%, S_{BET} = 35.7 $m^2\ g^{-1}$) was first impregnated with an aqueous solution of $(NH_4)_6Mo_7O_{24}{\cdot}4H_2O$ (99.98%, Aldrich) and then dried overnight in air at 400 K and calcined at 773 K in flowing air for 4 h to produce a supported oxide denoted here as MoO_3/MgO. Carburization of MoO_3/MgO was accomplished by temperature-programmed reaction (TPR) at temperatures between 673 K and 973 K with a 20 vol.% CH_4 (GTS-Welco, 99.997%) and 80 vol.% H_2 mixture (GTS-Welco, 99.999%) at a heating rate of 0.5 K min^{-1}, according to the method described by Woo et al. [17]. After TPR, the temperature was maintained at 973 K for 5 h, followed by another 10 h at 773 K. The catalyst was subsequently quenched to room temperature in flowing H_2. Finally, the 5 wt.% Mo_2C/MgO sample was passivated in a stream of 1 vol.% O_2/N_2 mixture (GTS-Welco, 1.02 vol.% O_2) at room temperature (RT) for 12 h before exposure to air. The supported Mo_2C was further promoted by grinding Rb_2CO_3 (99.975%, Alfa Aesar) together with the catalyst using a mortar and pestle. The Rb_2CO_3 loading was varied in the range of 0–15 wt.%.

As a control, distilled, deionized water was added to pure MgO, and the resulting sample was subjected to the same carburization conditions as samples containing Mo.

2.2. Catalyst characterization

Elemental analyses were performed by Galbraith Laboratories (Knoxville, TN). The Mo loading of the catalysts was determined by inductively coupled plasma atomic emission spectroscopy (ICP-AES), while the C loading was evaluated by combustion and colorimetric determination.

Adsorption of N_2 was performed on a Micromeritics ASAP 2020 automated adsorption system to obtain the BET surface area. A sample was heated under vacuum to 573 K for 10 h prior to adsorption of N_2 at liquid nitrogen temperature.

Electron microscopy was performed on an FEI Titan 300 transmission electron microscope equipped with an EDS system operated at 200 kV. Two catalyst samples, 5 wt.% Mo_2C/MgO and 5 wt.% Rb–5 wt.% Mo_2C/MgO, were reacted for 48 h and passivated with 1% O_2/N_2 (GTS-Welco, 1.02%O_2) at RT before TEM analysis. Catalyst powders were dispersed in *n*-hexane and supported onto a holey carbon film and a continuous carbon film (double film)-coated grid (Pacific Grid-Tech). Images were recorded with a Gatan 794 Multi Scan CCD camera and Fischione Instruments Model 3000 annular dark field detector.

The X-ray diffraction patterns were obtained on a Scintag XDS 2000 diffractometer using Cu Kα radiation. Scans were collected from 2θ of 5° to 90° at a rate of 2° min^{-1} for bulk materials and 0.8° min^{-1} for supported catalysts.

2.3. Higher alcohol synthesis

Hydrogenation of CO was conducted in a fixed-bed stainless steel reactor (BTRS Jr., Autoclave Engineers) with 1.00 g catalyst (0.05 g nominal Mo_2C) of size 40–80 mesh diluted by 2.5 g SiC. The catalysts were tested at nominally identical conditions of 573 K, 30 bar total pressure, syngas (H_2 + CO) flow of 20 $cm^3\ min^{-1}$ (STP), and H_2:CO ratio of 1:1. The reactor was pressurized to 30 bar at room temperature and heated to 573 K before sampling. The temperature of the catalyst bed was monitored by a thermocouple in contact with the catalyst bed. The purity of CO (GT&S) was 99.9% and that of H_2 (GT&S) was 99.999%. Additionally, CO was purified by passing it through a silica trap immersed in a dewar containing a dry ice/acetone mixture (195 K) to remove any trace iron carbonyl before introduction into the reactor [28]. The products were analyzed by two Hewlett–Packard 5890 series II gas chromatographs. The first one was equipped with a flame ionization detector and a 50-m-long HP-1 cross-linked methyl silicone gum capillary column to monitor the formation of hydrocarbons and oxygenates. The second one was equipped with a thermal conductivity detector

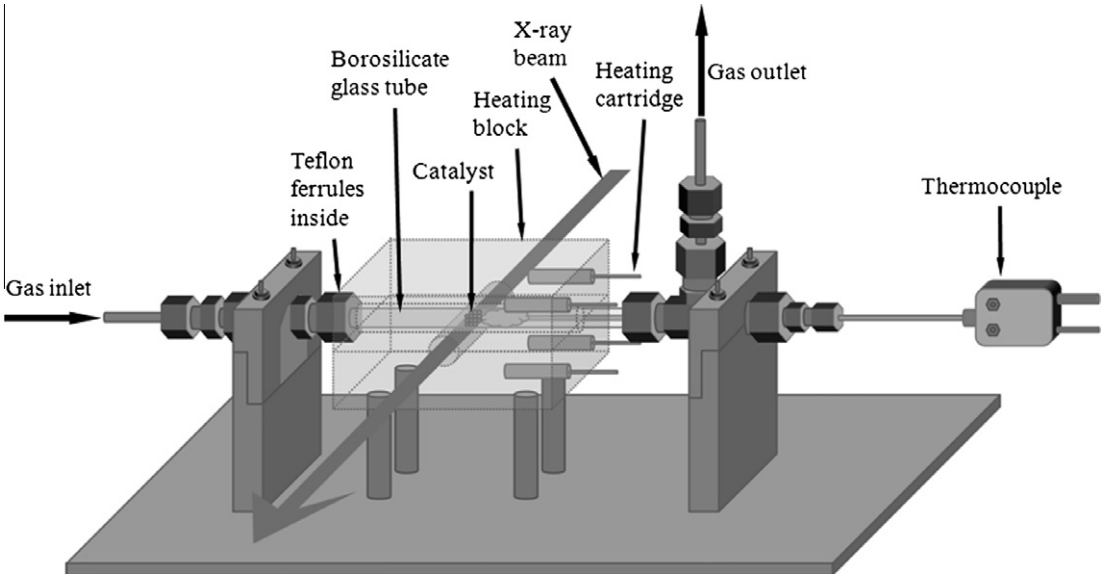

Fig. 1. High pressure, borosilicate tubular reactor/X-ray cell.

and a 6-ft-long Alltech-8700 packed column and was used to monitor the formation of CO_2.

According to Burch and Petch [29], the conversion of CO was derived from the fraction of CO that formed carbon-containing products. The conversion of CO, if low, can be described as:

$$\text{Conversion } (\%) = \sum n_i M_i \times 100/M_{CO},$$

where n_i is the number of carbon atoms in product i, M_i is the percentage of product i detected, and M_{CO} is the percentage of CO in the syngas feed.

The selectivity to product i is based on the total number of carbon atoms in the product and is therefore defined as:

$$\text{Selectivity} = n_i M_i / \sum n_i M_i.$$

2.4. X-ray absorption spectroscopy

X-ray absorption spectroscopy (XAS) was carried out on beamline X-18B at the National Synchrotron Light Source, Brookhaven National Laboratory. The NSLS storage ring was operated at 2.8 GeV with a ring current of about 300 mA. The XAS data were obtained in the transmission mode at the Mo K edge (20 keV) and at the Rb K edge (15.2 keV) with a spot size of 0.5 mm × 3 mm.

Following the designs of Fingland et al. [30], an XAS cell depicted in Fig. 1 was constructed in house specifically for this study. The XAS cell consists of a 6-in. borosilicate glass tube (1/4 in. OD, 5/32 in. ID) housed by stainless steel nuts and Teflon ferrules in a temperature-controlled aluminum heating block, with a ¼-in. hole in the block to allow for the transmission of X-rays through the tube walls and the catalyst bed. The temperature of the catalyst bed was controlled by an internal K-type stainless steel thermocouple (Omega). The heat to the aluminum block was provided by four ¼-in. cartridge heaters connected to an Omega CN 2011 temperature controller. The cell allowed for the interrogation of the catalyst under standard reaction conditions of 573 K and 30 bar flowing syngas.

The Mo K edge and Rb K edge spectra were measured in air at RT with Mo foil (0.015 mm, 99.9%, Goodfellow) and Rb_2CO_3 (99.975%, Alfa Aesar) as references, respectively. For in situ experiments, 0.2 g of 5 wt.% Mo_2C/MgO or 5 wt.% Rb–5 wt.% Mo_2C/MgO was loaded into a reactor tube and assembled into the custom-designed XAS cell. After pressurizing the cell with syngas ($CO:H_2$ = 1:1), it was then heated from RT to 573 K and held at 573 K for 4 h, with a total syngas flow of 4 $cm^3\ min^{-1}$ (STP). The Mo K edge and Rb K edge spectra were recorded after the 4-h treatment under reaction conditions and after quenching the catalysts to RT in H_2.

To further probe the Rb K edge, 0.2 g of 5 wt.% Rb–5 wt.% Mo_2C/MgO or 5 wt.% Rb/MgO was loaded into a reactor tube and assembled into the cell. The cell was then heated from RT to 573 K and held at 573 K for 4 h, in flowing Ar at 4 $cm^3\ min^{-1}$. The Rb K edge spectra were recorded after the 4-h treatment and after cooling the catalyst to RT in Ar. In addition, Rb K edge spectra of Rb_2CO_3 mixed with liquid water at RT were recorded.

The XAS data were processed using the Athena [31] software for background removal, post-edge normalization, and X-ray absorption near edge structure (XANES) analysis. Because the Mo near edge structure has various features that complicate the determination of E_0, the edge energy, the value of E_0 was assigned here as the energy at the half step height. Metallic Mo foil (0.015 mm, 99.9%, Goodfellow), MoO_2 (99%, Aldrich), and Rb_2MoO_4 (99.5%, Alfa Aesar) were used as standards for Mo residing in 0, +4, and +6 formal oxidation states.

The extended X-ray absorption fine structure (EXAFS) data analysis was performed using the Artemis software package, which implemented FEFF6 [31,32]. The normalized EXAFS data were k^3-weighted and then Fourier-transformed from k-space in the range 2–14 $Å^{-1}$. Standard bulk Mo_2C (Aldrich, 99.5%) was used to determine the amplitude reduction factors S_0^2 for Mo–C and Mo–Mo, and Rb_2MoO_4 was used to determine S_0^2 for Mo–O. The values of S_0^2 utilized in the fitting of EXAFS data from the catalyst samples were 0.82, 0.78, and 0.79 for Mo–C, Mo–Mo, and Mo–O, respectively. A two-shell fitting procedure was used to analyze carbides (Mo–C and Mo–Mo), and a one-shell fitting procedure was used to analyze the oxides (Mo–O). The interatomic distances (r), coordination numbers (CN), Debye–Waller factors (σ^2), and energy shifts (ΔE_0) were derived from the results.

3. Results and discussion

3.1. Characterization by X-ray diffraction, elemental analysis, N_2 adsorption, and electron microscopy

The X-ray diffraction patterns of representative samples are provided in Fig. 2. The pattern for bulk Mo_2C prepared at 973 K (Fig. 2c) revealed peaks at 34.8, 38.2, 39.8, 62.1, and 75.2°, which are assigned to the {1 0 0}, {0 0 2}, {1 0 1}, {1 1 0}, and an unresolved doublet of the {1 1 2} and {2 0 1} reflections of bulk β-Mo_2C, respectively [33]. The passivated 5 wt.% Mo_2C/MgO catalyst (Fig. 2b) prepared at 973 K showed XRD peaks corresponding to the structure of MgO (Fig. 2a) without any clear evidence for crystalline Mo_2C. This result suggests that the Mo_2C particles were very well dispersed on the support. It should be noted that MgO reconstructed to $Mg(OH)_2$ (Fig. 2d) after impregnation with a water solution followed by drying. However, after calcination at 773 K, the original pattern for MgO was restored. The significant reconstructing of the MgO support during catalyst preparation may have influenced the dispersion of the Mo on the surface.

The elemental analysis results for Mo_2C/MgO are listed in Table 1. Since MgO can adsorb CO_2 from air, a control experiment was carried by using a "carburized" MgO sample that was exposed to the same treatment as the catalyst synthesis except that no molybdenum precursor was added. The measured carbon level in the Mo_2C/MgO catalyst was then corrected by the carbon level in the control sample without Mo to give a more reliable analysis. The corrected C/Mo atomic ratio was 0.424, which is close to the expected stoichiometry of Mo_2C (0.5). The small deviation may be caused by the passivation step which may oxidize some of the surface carbon on the sample.

Table 2 lists the results of BET surface area analysis of MgO and MgO-supported Mo_2C catalysts prior to use in reaction. The BET

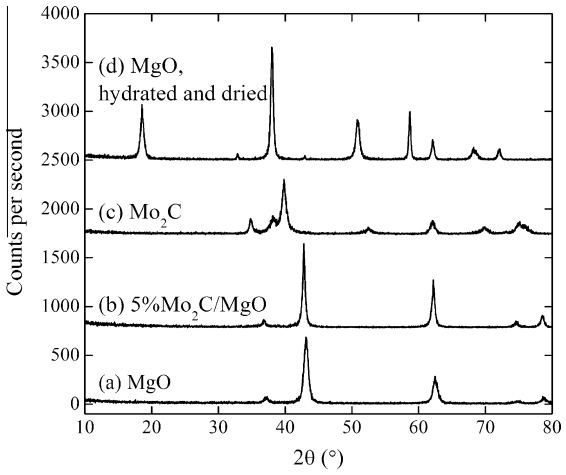

Fig. 2. X-ray diffraction patterns of: (a) MgO, (b) Mo_2C/MgO, (c) Mo_2C, and (d) hydrated MgO. Patterns are offset for clarity.

Table 1
Results from elemental analysis used to determine stoichiometry for Mo_2C/MgO catalysts.

Catalyst composition (nominal)	Loading (wt.%)		C/Mo (atomic ratio)	
	Mo	C	Measured	Corrected
5 wt.% Mo_2C/MgO	4.77	0.356	0.596	0.424[a]
"Carburized" MgO	–	0.108	–	–

[a] Value has been corrected by the level in "carburized" MgO.

Table 2
Results from N_2 adsorption.

Sample	S_{BET} ($m^2\ g^{-1}$)
MgO	35.7
5% Mo_2C/MgO	64.8
1%Rb–5%Mo_2C/MgO	65.7
5%Rb–5%Mo_2C/MgO	55.4
10%Rb–5%Mo_2C/MgO	54.2
15%Rb–5%Mo_2C/MgO	48.4

surface area of MgO changed from 35.8 $m^2\ g^{-1}$ to 64.8 $m^2\ g^{-1}$ after loading with Mo_2C. Considering the small proportion of Mo_2C on the sample, the change in the BET surface area of MgO most likely was the result of the structure change of MgO to $Mg(OH)_2$ and back to MgO during catalyst synthesis. Addition of a high loading of Rb_2CO_3 to the sample by physically mixing the two components decreased the overall area of the mixture, as expected.

The high angle annular dark field (HAADF) image of 5 wt.% Mo_2C/MgO (Fig. 3) revealed that the average particle size of Mo_2C was 2.8 ± 0.3 nm. The very small particle size observed by TEM is consistent with the lack of observable crystalline carbide phases by X-ray diffraction.

3.2. Role of Rb loading on Mo_2C/MgO

The performance of unpromoted Mo_2C catalysts in the reaction of syngas ($CO:H_2$ = 1:1) at 573 K and 30 bar pressure is summarized in Table 3.

The first two entries in Table 3 compare the results from a bulk Mo_2C catalyst and an MgO-supported Mo_2C catalyst. Bulk Mo_2C functions primarily as a Fischer–Tropsch catalyst at 573 K and 30 bar syngas, producing mainly light hydrocarbons and very little alcohols (2.9% on a CO_2-free basis). Supporting the carbide on MgO increased the alcohol selectivity to 22%, at a similar level of CO conversion. Evidently, the basic support MgO promoted alcohol production at the expense of hydrocarbon production, most likely at active sites near the carbide/support interface. It should be noted that the selectivity to CO_2 produced via the water gas shift reaction was usually about 40% and should always be below 50% because of reaction stoichiometry.

To explore the role of support basicity on reactivity, 5 wt.% Mo_2C was prepared on α-alumina (Mager Scientific AP332) using identical conditions to synthesize the MgO-supported carbides. The alumina-supported carbide was very highly dispersed since no peaks in the X-ray diffraction pattern could be attributed to Mo_2C. The 5% Mo_2C/α-alumina catalyst produced 94% hydrocarbons (0.6% alcohols) at 7.1% CO conversion, whereas 5% Mo_2C/MgO produced 71% hydrocarbons (22% alcohols) at 6.0% CO conversion (Table 3), which suggests that the basicity of MgO facilitates alcohol production on the supported carbides.

Entries 3–7 in Table 3 illustrate the effect of Rb loading on higher alcohol synthesis over Mo_2C/MgO. Addition of Rb_2CO_3 to supported Mo_2C increased the selectivity to alcohols (on a CO_2-free basis) while lowering the selectivity to hydrocarbons. However, the addition of Rb_2CO_3 beyond 10 wt.% did not substantially improve selectivity above about 60% oxygenates but instead decreased CO conversion. Examination of the distribution of alcohols produced over the catalysts shows that the ratio of higher alcohols (ethanol, propanol, etc.) to methanol was nearly 1:1 over unpromoted Mo_2C/MgO but was 2.4 over Rb-promoted Mo_2C/MgO. Moreover, the addition of Rb promoted the formation of alkenes, because the C4+ alkene/C4+ alkane ratio increased from 0.47 on unpromoted 5 wt.% Mo_2C/MgO to 2.1 on 10 wt.% Rb–5 wt.% Mo_2C/MgO. These results are consistent with prior work on potassium-promoted bulk Mo_2C catalysts [17,34,35]. In summary, the addition of Rb promoter to Mo_2C/MgO decreased the rate of CO conversion and simultaneously increased the alcohol productivity (Table 3) for Rb loadings up to about 10 wt.%. In contrast, a high loading of Rb (15 wt.%) actually decreased alcohol productivity presumably by blocking active sites on the catalyst.

The fourth and fifth entries in Table 3 demonstrate the reproducibility of the reactivity results by reporting two separate runs of 5 wt.% Rb–5 wt.% Mo_2C/MgO catalysts. The results suggest good experimental reproducibility since the conversion of CO (3.5% and 3.0%) and product distribution are very similar.

Fig. 4 illustrates how the CO conversion and product selectivities over 5 wt.% Rb–5 wt.% Mo_2C/MgO changed with time over a 48-h time interval. The catalyst deactivated about a third of its initial activity after about 24 h but remained fairly stable thereafter. The selectivity to hydrocarbons, alcohols, and CO_2 all changed sharply during the first 3 h and was relatively stable after about a day. Most importantly, the alcohol selectivity was very low initially and gradually increased with time on stream, suggesting a

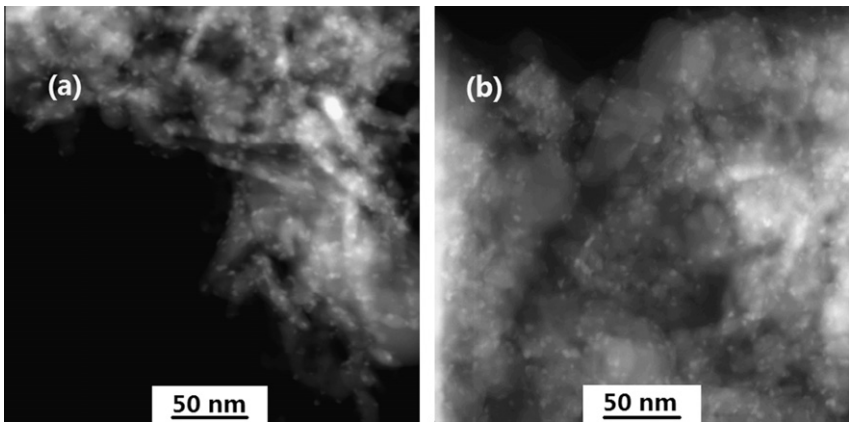

Fig. 3. HAADF images of: (a) 5% Mo_2C/MgO and (b) 5%Rb–5%Mo_2C/MgO. Catalysts had been used for 48 h in CO hydrogenation before TEM analysis.

Table 3
Conversion of synthesis gas over Rb-promoted 5 wt.% Mo_2C/MgO catalysts.

Catalyst	CO conv. (%)	Rate of CO conv. (mol mol_{Mo}^{-1} h^{-1})	CO_2 sel. (%)	Selectivity (C% on a CO_2-free basis) [a]											Rate of alcohol production (g g_{Mo}^{-1} h^{-1})
				CH_4	$C_2H_6 + C_2H_4$	$C_3H_8 + C_3H_6$	C_nH_{2n+2} ($n > 3$)	C_nH_{2n} ($n > 3$)	MeOH	EtOH	PrOH	BuOH	PeOH	Esters [b]	
Bulk Mo_2C	6.9	3.5	43	38	25	19	5.0	2.6	1.9	1.0	0.0	0.0	0.0	7.8	0.017
5%Mo_2C/MgO	6.0	3.0	43	27	21	15	5.5	2.6	11	7.5	3.2	0.0	0.0	7.3	0.11
1%Rb–5%Mo_2C/MgO	3.9	2.0	45	18	15	12	7.4	4.2	14	15	6.6	1.7	0.0	6.0	0.11
5%Rb–5%Mo_2C/MgO	3.5	1.8	38	16	12	7.7	3.2	4.4	18	22	10	2.9	0.0	2.3	0.16
5%Rb–5%Mo_2C/MgO	3.0	1.5	37	15	9.8	6.1	3.1	5.1	19	22	12	4.1	1.8	1.4	0.14
10%Rb–5%Mo_2C/MgO	2.8	1.4	35	16	10	6.0	1.9	3.9	18	23	14	4.2	1.8	0.8	0.14
15%Rb–5%Mo_2C/MgO	2.3	1.1	39	16	10	5.9	1.6	4.0	18	23	16	4.5	0.0	0.0	0.11

Notes: Nominal conditions are $T = 573$ K, $P = 30$ bar, 0.05 g nominal Mo_2C (made into 40–80 mesh pellets if supported on MgO), 2.5 g SiC to dilute the bed, H_2:CO 1:1, syngas flow = 20 cm^3 min^{-1} (STP). Data were recorded after 48-h reaction. Conversion (%) = $\sum n_i M_i \times 100/M_{CO}$ and selectivity = $n_i M_i/\sum n_i M_i$, where n_i is the number of carbon atoms in product i, M_i is the mole percent of product i measured, and M_{CO} is the mole percent of carbon monoxide in the feed. The quantitative products comprised more than 93% of the total peak area given by GC-FID.

[a] All the alcohols are linear.

[b] Esters include methyl formate and methyl acetate.

restructuring of the active phase during this start-up period. Generally, molybdenum-based catalysts for mixed alcohol synthesis exhibit an induction period during CO hydrogenation [16,28–31]. This induction period may coincide with the distribution of Rb promoter over the catalyst surface since it was initially physically mixed with Mo_2C/MgO.

Lee et al. [18] depicted the simplified scheme (Scheme 1) of CO conversion based on the ideas discussed by Ponec et al. [36,37]. According to this scheme, all products can be derived from an adsorbed intermediate $^*C_mH_n$, (where $*$ denotes a surface site). This intermediate can undergo four different transformations to products, namely (1) hydrogenation to alkanes, (2) carbonylation to alcohol precursors, (3) desorption as olefins and (4) further chain growth by inserting $^*CH_x$. In this competitive process, hydrogenation activity of a catalyst needs to be partially suppressed to enhance the production of alcohols and alkenes; thus, trends in alcohol and alkene selectivities should be similar, as reaction conditions or catalyst properties are varied. Lee et al. [18] suggested that alkali promoters on Mo_2C catalysts for CO hydrogenation have two effects: an electronic effect and a geometric effect. The electronic effect is thought to increase the electron density of the catalyst, thus inhibiting the oxidative addition of hydrogen to the surface. The geometric effect involves the blockage of surface sites that are potential sites for the adsorption of reactants. They concluded that the geometric effect of adding K_2CO_3 on Mo_2C was the primary mode of promoting alcohol formation during CO hydrogenation. Because the optimal ratio of K to Mo was different for alkene and alcohol formation, Lee et al. also suggested that alkene formation may be attributed to the combination of geometric and electronic effects. Muramatsu et al. [38] also studied the roles of potassium promoter on a Mo oxide catalyst for alcohol production from syngas and concluded that potassium inhibits the dehydration of alcohols to alkenes as well as the hydrogenation of alkenes to alkanes.

For CO hydrogenation over Mo_2C/MgO catalysts, the selectivities of both alcohols and alkenes increased with the loading of Rb_2CO_3 promoter, which is consistent with Scheme 1. The EDS spectra of 5 wt.% Rb–5 wt.% Mo_2C/MgO catalyst after 48-h syngas reaction, corresponding to the sample in Fig. 3b, revealed the presence of Rb distributed over the sample after reaction, which is consistent with a site blocking mechanism described above. However, the formation of higher alcohols with increased loading of Rb promoter may result from chain growth reactions on the promoted carbide catalyst or coupling of lower molecular weight alcohols over basic sites provided by Rb promoter. Further investigations are needed to explore this aspect.

3.3. Influence of process variables: gas flow rate, temperature, pressure, and H_2:CO ratio

The influence of gas flow rate on the overall CO conversion is shown in Fig. 5 at the nominal conditions of 30 bar and a H_2/CO ratio of 1, with temperature varying from 553 K to 593 K. As expected, CO conversion decreased with gas flow rate and increased with temperature.

Table 4 compares the behavior of 5 wt.% Rb–5 wt.% Mo_2C/MgO at the same pressure (30 bar) and same CO conversion level by varying gas flow rate and temperature. The selectivity of alcohols was independent of temperature over the range of 573–593 K at a constant conversion of CO equal to about 2.8% (excluding CO_2). However, the selectivity to alcohols and hydrocarbons is a strong function of CO conversion, as revealed in Fig. 6. At 30 bar, alcohol formation is preferred at low CO conversion, which is also observed over alkali-promoted, MoS_2-based catalysts for higher alcohol synthesis [39].

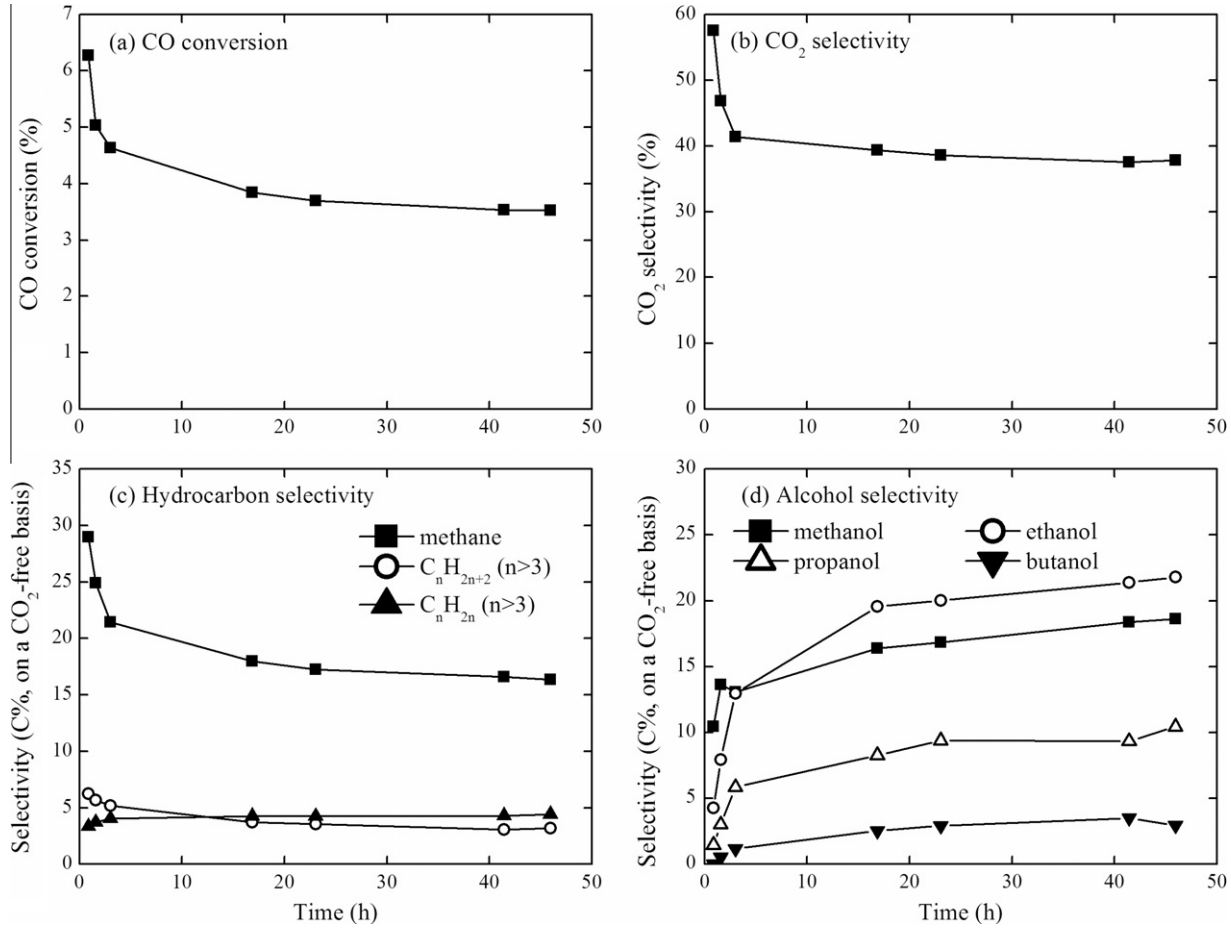

Fig. 4. Change in catalytic performance of 5 wt.% Rb–5 wt.% Mo_2C during CO hydrogenation at 573 K and 30 bar: (a) CO conversion; (b) selectivity to CO_2; (c) selectivity to hydrocarbons; (d) selectivity to alcohols.

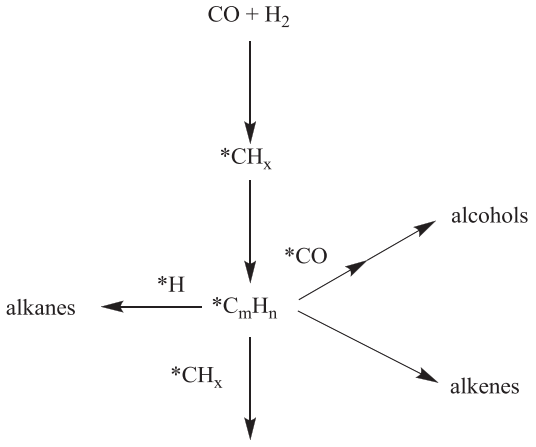

Scheme 1. Reaction pathway for CO hydrogenation adapted from [18].

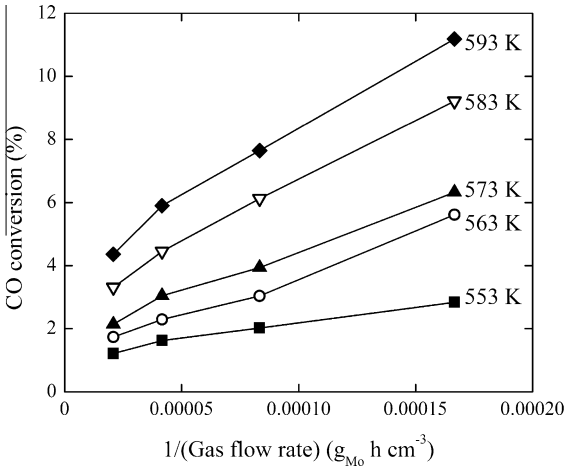

Fig. 5. Influence of gas flow rate on CO conversion (including CO_2) over 5 wt.% Rb–5 wt.% Mo_2C/MgO (30 bar, H_2/CO = 1).

Table 5 summarizes the effect of reactant partial pressures on the CO conversion and product selectivity over 5 wt.% Rb–5 wt.% Mo_2C/MgO at 573 K. The results indicate that the overall reaction is positive order in H_2 but is inhibited by CO at the tested conditions. The changes in conversion during the various runs in Table 5 account for observed changes in alcohol and hydrocarbon selectivity.

Table 6 presents the influence of total syngas pressure on the CO conversion and selectivity of CO hydrogenation over 5 wt.% Rb–5 wt.% Mo_2C/MgO at 573 K with CO:H_2 of 1 at a total flow rate of 20 cm^3 (STP) min^{-1}. The CO conversion increased with pressure over the range of 10–30 bar while simultaneously the selectivity to higher alcohols slightly improved from 37% to 41%.

3.4. X-ray absorption spectroscopy

The X-ray absorption near edge structure (XANES) at the Mo *K* edge of reference compounds and catalysts is provided in Fig. 7,

Table 4
Comparison of catalyst activity at similar CO conversion level by varying temperature and gas flow rate.

CO conversion (%)	4.2	4.5	4.4
CO_2 selectivity (%)	37	37	36
CO conv. (%, excluding CO_2)	2.7	2.8	2.8
Pressure (bar)	30	30	30
Temperature (K)	573	583	593
CO:H_2	1	1	1
Gas flow rate ($cm^3\ g_{Mo}^{-1}\ h^{-1}$)	12,000	24,000	48,000
Selectivity (C%, on a CO_2-free basis)			
CH_4	16	17	18
$C_2H_6 + C_2H_4$	11	11	12
$C_3H_8 + C_3H_6$	6.9	6.7	6.8
C_nH_{2n+2} ($n > 3$)	3.7	3.1	2.2
C_nH_{2n} ($n > 3$)	5.1	4.9	5.3
MeOH	17	18	17
EtOH	20	20	20
PrOH	12	11	11
BuOH	3.8	3.6	4.0
PeOH	1.6	1.4	1.8

Table 5
Impact of partial pressure on production distribution of CO hydrogenation over 5 wt.% Rb–5 wt.% Mo_2C/MgO catalyst.

Temperature (K)	573	573	573
Partial pressure (bar)			
CO	7.5	15	15
H_2	15	15	7.5
$H_2 + CO$ ($cm^3\ min^{-1}$)	15	20	15
CO conversion (%)	4.9	3.2	2.1
Rate of conversion (mol $g_{Mo}^{-1}\ h^{-1}$)	0.024	0.016	0.010
CO_2 selectivity (%)	30	34	28
Selectivity (C%, on a CO_2-free basis)			
Hydrocarbons	45	39	41
CH_4	20	15	15
$C_2H_6 + C_2H_4$	12	10	12
$C_3H_8 + C_3H_6$	6.7	5.9	6.6
C_nH_{2n+2} (C > 3)	3.0	3.2	2.1
C_nH_{2n} (C > 3)	3.6	4.8	5.1
MeOH	21	19	20
Higher alcohols	32	41	38
EtOH	19	22	21
PrOH	8.5	12	12
BuOH	2.7	4.1	4.0
PeOH	1.0	1.8	1.6

and a correlation of edge position of the samples (determined at half step height) with the oxidation state of standard Mo compounds is illustrated in Fig. 8. The edge position of a sample prior to carburization indicated that calcined Mo on MgO was in a +6 oxidation state. Carburization resulted in significant reduction of Mo, which is consistent with the formation of a carbide surface compound. Bulk Mo_2C showed a slightly higher absorption edge energy than Mo foil (Figs. 7a and 8), but the Mo in Mo_2C was significantly reduced from that in MoO_2. The absorption edge of passivated 5 wt.% Mo_2C/MgO catalyst before reaction was shifted +1.8 eV from bulk Mo_2C (Fig. 7b), but was still 1.5 eV lower than the edge position of MoO_2, which indicates the supported Mo_2C

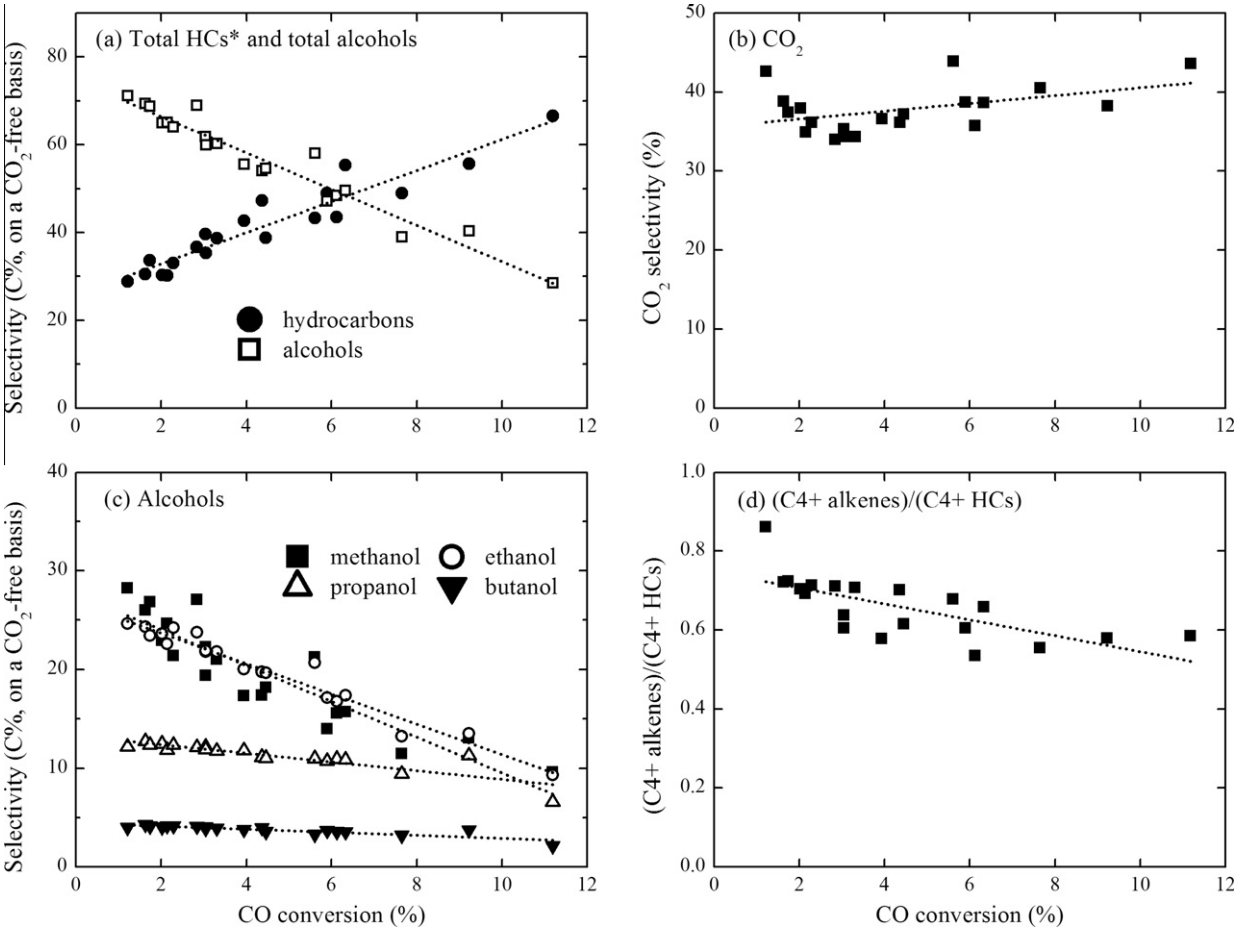

Fig. 6. Influence of CO conversion on product distribution during HAS over 5 wt.% Rb–5 wt.% Mo_2C/MgO over a temperature range of 553–593 K: (a) selectivity of total hydrocarbons and total alcohols; (b) selectivity of CO_2; (c) selectivity of individual alcohols; (d) ratio of alkenes and alkanes. * HC refers to hydrocarbon.

Table 6
Effect of pressure on HAS over a 5 wt.% Rb–5 wt.% Mo_2C/MgO catalyst.

Pressure (bar)	10	20	30
Temperature (K)	573	573	573
CO:H_2	1	1	1
H_2 + CO (cm^3 min^{-1})	20	20	20
CO conversion (%)	1.9	2.9	3.6
CO_2 selectivity (%)	32	38	41
Selectivity (C%, on a CO_2-free basis)			
Hydrocarbons	43	38	39
CH_4	17	16	15
C_2H_6 + C_2H_4	12	11	9.6
C_3H_8 + C_3H_6	6.8	5.8	5.9
C_nH_{2n+2} (C > 3)	1.5	1.7	3.2
C_nH_{2n} (C > 3)	5.0	4.2	4.8
MeOH	19	21	19
Higher alcohols	37	39	41
EtOH	21	22	22
PrOH	10	11	12
BuOH	3.3	4.1	4.1
PeOH	1.4	1.7	1.8

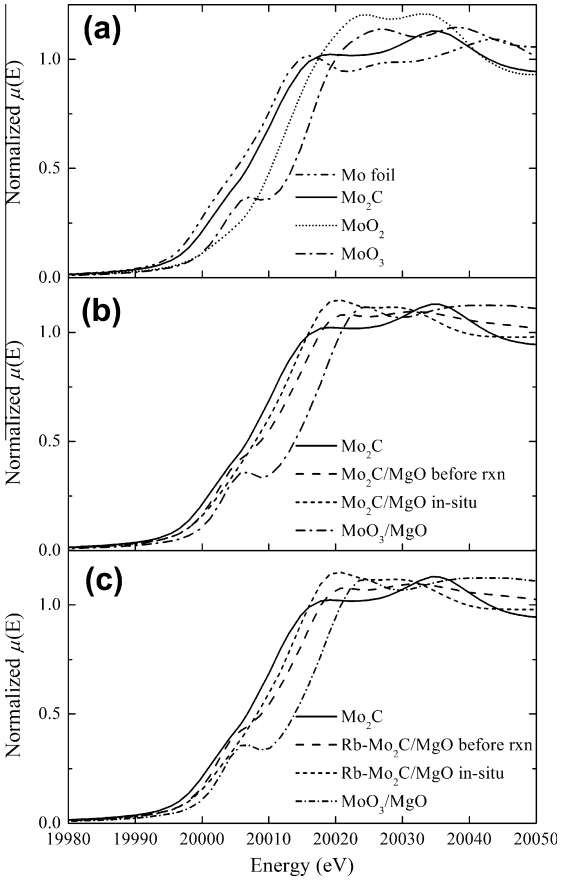

Fig. 7. X-ray absorption near edge structure (XANES) at the Mo *K* edge of: (a) Mo reference standards, (b) Mo_2C/MgO, (c) Rb–Mo_2C/MgO. MoO_3/MgO is the catalyst precursor before carburization.

catalysts were partially oxidized, with the surface of the Mo_2C particles likely being an oxycarbide. Most probably, passivation of the freshly prepared carbide catalysts is responsible for the oxidation. The in situ treatment of Mo_2C/MgO catalysts in 30 bar syngas at 573 K for 4 h partially reduced the passivated 5 wt.% Mo_2C/MgO (Figs. 7 and 8), but the Mo was still more oxidized than in bulk Mo_2C (Fig. 8). The small shifts in E_0 illustrated in Fig. 8 caused by the addition of Rb_2CO_3 to the corresponding unpromoted Mo_2C/MgO were within the experimental error.

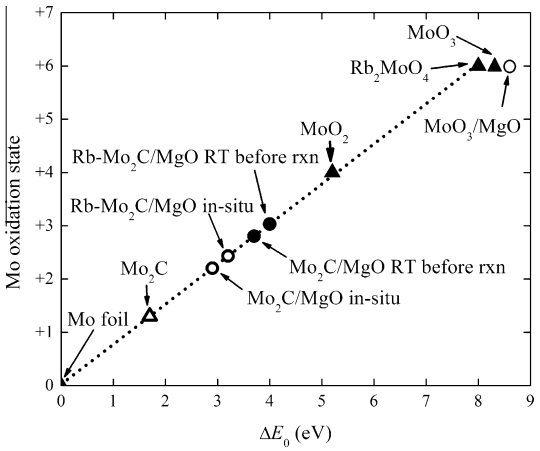

Fig. 8. Correlation of the Mo *K* edge energy (E_0 defined as energy at half step) with the oxidation state of reference compounds (triangles) and supported catalyst (circles).

The shift of the Mo *K* edge to lower energy during the induction period of the reacting catalyst was likely caused by the removal of surface oxygen atoms that were introduced by passivation. Griboval-Constant et al. suggested that part of the surface oxygen introduced by passivation of β-Mo_2C probably reacted with carbidic carbon, which was removed from the uppermost surface layer during this induction period [40]. Ranhotra et al. hypothesized that the removal of surface oxygen during the induction period must be coincident with the elimination of some surface carbon because oxygen atoms are more strongly bonded to Mo than carbon [41]. Clearly, the passivation layer on Mo_2C can significantly affect the surface structure of the catalyst. Wu et al. observed that fresh β-Mo_2C had many more sites for CO adsorption than a passivated sample, and few of the passivated sites could be recovered by H_2 reduction at 673 K and 773 K. From our XANES results, we conclude that the passivated sites on Mo_2C/MgO catalysts could not be fully recovered since Mo remained partially oxidized in situ.

Fourier transforms of the Mo *K* edge extended X-ray absorption fine structure (EXAFS) are presented in Fig. 9. The coordination numbers (CN), interatomic distances (r), and Debye–Waller factors (σ^2) obtained by curve fitting are summarized in Table 7. Example curve fits associated with the results in Table 7 are compared with the experimental EXAFS for Mo *K* edge EXAFS of 5 wt.% Rb–5 wt.% Mo_2C/MgO (treated in situ for 4 h) in Fig. 10. All of the R-factors of the fits are around 0.1 or much less.

The Mo EXAFS of the MoO_3/MgO sample (Fig. 9f) before carburization was quite different from bulk MoO_3 (Fig. 9h). No Mo–Mo interaction was observed in the supported sample, and the Mo–O distance appeared to be contracted from the bulk oxide. The lack of Mo–Mo contributions indicates that Mo was very highly dispersed on the MgO support. Indeed, $(NH_4)_6Mo_7O_{24}$ precursor solution reacted with the MgO support during catalyst preparation because the odor of ammonia was detected during wet impregnation. In the EXAFS analysis, the Mo–O distance in MoO_3/MgO was exactly the same as that in Rb_2MoO_4, which suggests that our precursor of Mo_2C supported on MgO might be a surface Mg molybdate, although we refer to the sample as MoO_3/MgO.

Contributions from Mo–Mo in the Mo EXAFS of the Mo_2C catalysts were observed after carburization of the MoO_3/MgO sample in CH_4/H_2. It should be noted that the low intensity of the Mo–Mo peaks in the Fourier transform of the carburized catalysts in Fig. 10 was partly the result of a lower coordination number (CN = 8–9, Fig. 10b and c) than that of the bulk β-Mo_2C standard (CN = 12, Fig. 10a). According to Jentys [42], the low Mo–Mo coordination numbers suggest that about 70% of the Mo atoms were

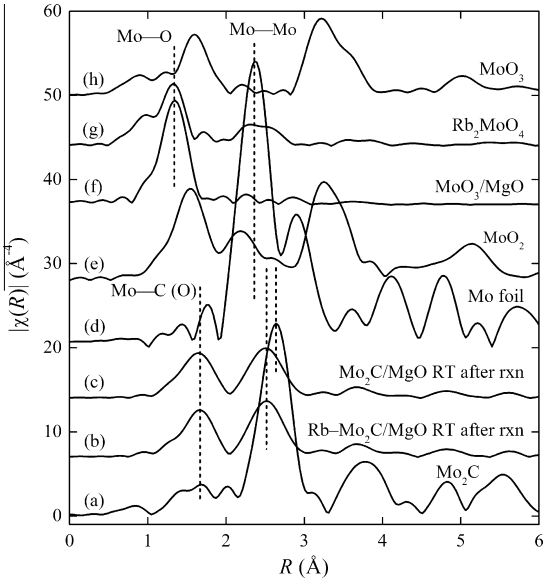

Fig. 9. Magnitude of the Fourier transform (not corrected for phase shifts) of the k^3-weighted Mo *K* edge EXAFS of Mo standards compared to MgO-supported Mo species: (a) Mo_2C, (b) Rb–Mo_2C/MgO RT after rxn, (c) Mo_2C/MgO RT after rxn, (d) Mo foil, (e) MoO_2, (f) MoO_3/MgO, (g) Rb_2MoO_4, (h) MoO_3. Transforms are offset for clarity.

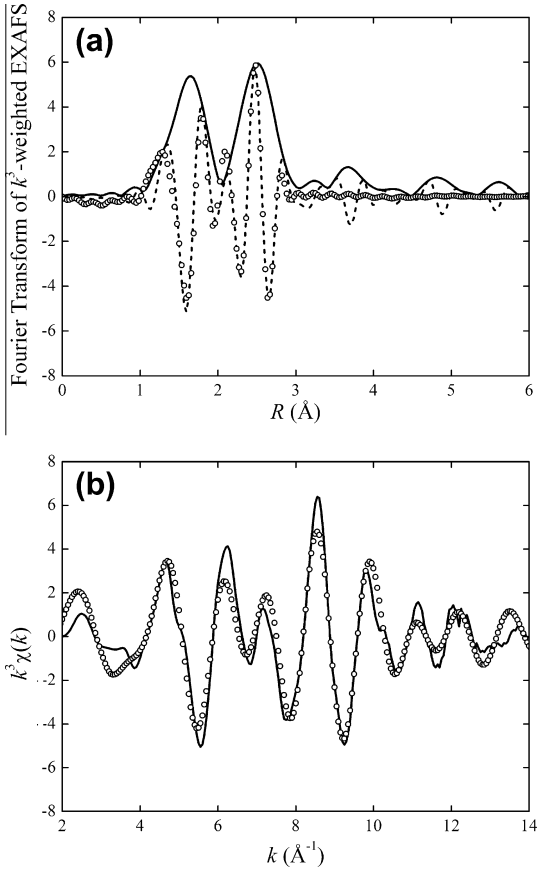

Fig. 10. Comparison of curve fit to experimental Mo *K* edge EXAFS of the 5 wt.% Rb–5 wt.% Mo_2C/MgO catalyst in 30 bar syngas at 573 K: (a) magnitude (solid line) and the imaginary part (dash line) of the Fourier transform of EXAFS compared with the result from the curve fit (circle); (b) k^3-weighted Mo *K* edge EXAFS (solid line) and the result from curve fit (circle).

exposed to the surface of the Mo_2C clusters, with a corresponding particle size of about 2 nm, which is slightly smaller than that derived from TEM analysis (2.8 ± 0.3 nm). This small difference could be the result of some particle aggregation observed in TEM and/or the shape of the Mo_2C clusters deviating from a perfect sphere. The ΔE_0 values (about −20 eV) need to fit the Mo–Mo contributions in the supported catalysts were much greater than those reported for Mo_2C supported on Al_2O_3 [11] and zeolite [43,44]. In Fig. 9, the Mo–Mo peak position in Mo_2C/MgO catalysts deviates about −0.12 Å from that in bulk β-Mo_2C and about +0.15 Å from metallic Mo. This shift might suggest the existence of metallic Mo in the Mo_2C/MgO catalyst. In fact, Lee and Boudart observed a Mo–Mo distance at 2.80 Å in Al_2O_3-supported metallic Mo [11], which is between bulk Mo metal (2.72 Å) and bulk β-Mo_2C (2.97 Å). However, results from XANES and elemental analysis both suggest the formation of carbidic Mo rather than metallic Mo. Therefore, we conclude that the Mo_2C/MgO catalysts have the local structure of carbidic Mo species, with a Mo–Mo distance (2.92 Å) contracted from the bulk β-Mo_2C (2.97 Å) because of the small particle size.

The Mo–C interaction in EXAFS of fresh supported Mo_2C catalysts has been studied elsewhere [11,43,44], and the coordination number of Mo–C varies from 0.6 to 2. In our study, the coordination numbers of the metal–nonmetal interactions in Mo_2C/MgO catalysts are all about 5, which exceed the value of 3 in the standard β-Mo_2C. Because the backscattering functions of C and O are similar, it was not possible to distinguish the different atom types in the EXAFS fitting. Considering the high percentage of surface Mo in Mo_2C/MgO catalysts, almost all surface Mo atoms will likely be bonded to oxygen atoms from passivation and could result in a high CN for the nonmetal. This speculation is consistent with the finding of Hwu et al. [45], who claim that an oxygen-modified

Table 7
Results from the analysis of Mo EXAFS.

Sample	Shell	CN	ΔE_0 (eV)	*r* (Å)	σ^2 (10^{-3} Å^2)	*R*-factor
Rb_2MoO_4	Mo–O	4[a]	7.4 ± 2.6	1.77 ± 0.01	2.5 ± 1.0	0.023
MoO_3/MgO	Mo–O	3.0 ± 0.4	1.8 ± 2.1	1.77 ± 0.01	3.8 ± 0.8	0.013
Mo_2C (bulk)	Mo–C (O)	3[a]	4.0 ± 3.5	2.12 ± 0.02	3.1 ± 2.0	0.005
	Mo–Mo	12[a]	−3.1 ± 0.8	2.97 ± 0.00	5.9 ± 3.8	
Mo_2C/MgO, in situ[b]	Mo–C (O)	5.1 ± 1.7	−2.5 ± 4.2	2.15 ± 0.02	6.2 ± 2.8	0.108
	Mo–Mo	7.8 ± 4.0	−25 ± 5	2.92 ± 0.02	13 ± 3	
Mo_2C/MgO, RT after rxn[b]	Mo–C (O)	5.3 ± 1.5	0.3 ± 3.5	2.16 ± 0.02	5.0 ± 2.2	0.068
	Mo–Mo	9.0 ± 3.2	−23 ± 3	2.93 ± 0.02	11 ± 2	
Rb–Mo_2C/MgO, in situ[b]	Mo–C (O)	5.1 ± 1.6	−2.6 ± 3.9	2.15 ± 0.02	6.0 ± 2.5	0.099
	Mo–Mo	8.2 ± 4.2	−26 ± 4	2.91 ± 0.02	14 ± 3	
Rb–Mo_2C/MgO, RT after rxn[b]	Mo–C (O)	5.8 ± 1.8	−2.4 ± 3.9	2.15 ± 0.02	5.7 ± 2.5	0.082
	Mo–Mo	8.5 ± 3.5	−24 ± 4	2.92 ± 0.02	11 ± 3	

In situ condition: *T* = 573 K, *P* = 30 bar, 0.2 g catalyst, H_2:CO = 1:1, syngas flow = 4 cm^3 min^{-1}; Fitting parameters: Fourier transform range Δk: 2–14 Å^{-1}; fitting range ΔR: 1–3 Å; weighting: k^3; S_0^2 (Mo–C) = 0.82, S_0^2 (Mo–Mo) = 0.78, S_0^2 (Mo–O) = 0.77.

[a] Value was assigned in curving fitting based on standard structure.

[b] Rbkg was set to 1.2 in background removal to remove the noise oscillation below 1 Å in *R* space.

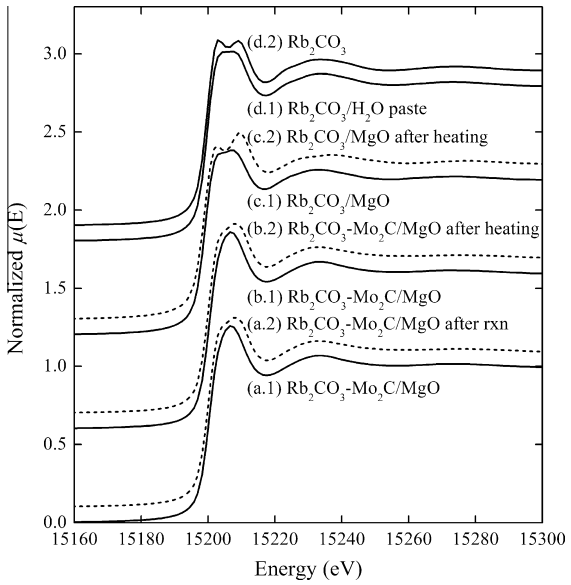

Fig. 11. XANES at the Rb *K* edge. Solid lines are spectra recorded at RT without any pretreatment. Dashed lines are spectra recorded at RT after various treatments: (a) Rb_2CO_3–Mo_2C/MgO (before and after exposure to 30 bar syngas at 573 K for 4 h), (b) Rb_2CO_3–Mo_2C/MgO (before and after heating in Ar at 573 K for 4 h), (c) Rb_2CO_3/MgO (before and after heating in Ar at 573 K for 4 h), (d.1) Rb_2CO_3/H_2O paste at RT, (d.2) Rb_2CO_3 as received. Spectra are offset for clarity.

Mo_2C surface can exist at 600 K. Although it is believed that some of the passivated Mo sites can be recovered by reduction to give sites for adsorption, the recovery could be fairly limited [33]. Moreover, even if some of the Mo sites are recovered, the reactant CO and adsorbed reaction intermediates could also contribute to the coordination environment around Mo. In summary, the high CN of nonmetal (C and O) in Mo_2C/MgO catalysts is a combination of carbidic carbon, oxygen coming from passivation, and the chemically adsorbed reaction intermediates, with a Mo–C (O) distance of 2.15 Å, which is slightly elongated from the Mo–C bonds in β-Mo_2C (2.12 Å).

Fig. 11 presents the near edge features of Rb species in different samples. The Rb_2CO_3 sample directly from the as-received bottle (Fig. 11d.2) has a double-peak near edge feature, which can be removed by hydration with a small amount of liquid water (Fig. 11d.1). Physically mixing Rb_2CO_3 with MgO or Mo_2C/MgO yielded a spectrum consistent with the hydrated sample (Fig. 11c.1 and d.1). As shown in Fig. 11c, heating of Rb_2CO_3/MgO in Ar regenerated the double peak feature that is similar to bulk Rb_2CO_3 in Fig. 11d.2. However, after heating the carbide sample in either Ar or syngas, the double peak edge structure of Rb_2CO_3 was not formed, which suggests a possible structural change in the Rb_2CO_3 on our active catalyst samples. Sarkar et al. observed similar Rb *K* edge spectra for rubidium-promoted Fischer–Tropsch catalysts, but concluded the promoter resembled Rb_2CO_3 based on a comparison to their different carbonate reference spectrum [46]. Additional studies are required to determine the nature of the supported Rb phase since the EXAFS above the Rb *K* edge was uninformative. We speculate that Mo may catalyze the decomposition of Rb_2CO_3 to more basic oxides or hydroxides. Earlier work in our laboratory showed that $BaCO_3$ decomposition was facilitated by H_2 in the presence of a transition metal such as Ru [47].

4. Conclusion

The synthesis of higher alcohols during CO hydrogenation reactions over Mo_2C/MgO catalysts at 30 bar and 573 K was promoted by both the basic support MgO and the presence of added Rb_2CO_3 promoter. Bulk β-Mo_2C was an effective Fischer–Tropsch catalyst under the standard conditions used here and produced only trace alcohols. Supporting Mo_2C onto MgO as 2- to 3-nm sized particles promoted the alcohol synthesis reaction, although hydrocarbons were still favored over alcohols. Addition of Rb_2CO_3 to Mo_2C/MgO substantially improved the selectivity to alcohols at the expense of hydrocarbons. Higher alcohol synthesis was favored at high syngas pressure and low CO conversion.

Results from X-ray diffraction, transmission electron microscopy, and X-ray absorption fine structure confirmed the high dispersion of Mo_2C on MgO. Near edge spectroscopy followed the incomplete reduction of passivated Mo_2C/MgO at reaction conditions and confirmed the presence of partially oxidized Mo during reaction. In situ EXAFS revealed that the Mo_2C clusters had a longer average Mo–C (O) interatomic distance (2.15 Å) and a shorter average Mo–Mo distance (2.92 Å) than bulk Mo_2C, presumably because of the high dispersion on MgO. The relatively large coordination of C (O) to Mo suggested the existence of surface oxycarbide layer on Mo_2C clusters. Electron microscopy and Rb *K* edge XANES indicated that Rb was well distributed over the surface but was chemically modified from bulk Rb_2CO_3.

Acknowledgments

The authors acknowledge financial support from The Dow Chemical Company and helpful discussion with collaborators at the Georgia Institute of Technology. The authors also acknowledge Dr. Mitsuhiro Murayama for acquisition of transmission electron micrographs and EDS analysis. Use of the NSLS was supported by the US Department of Energy, Office of Science, Office of Basic Energy Sciences, under Contract No. DE-AC02-98CH10886. Beamline X18B at the NSLS is supported in part by the Synchrotron Catalysis Consortium, US Department of Energy Grant No. DE-FG02-05ER15688. The authors acknowledge with gratitude the invaluable assistance received from the X-18B beam line personnel, Dr. Nebojsa Marinkovic and Dr. Syed Khalid.

References

[1] R.G. Herman, Catal. Today 55 (2000) 233.
[2] P. Forzatti, E. Tronconi, I. Pasquon, Catal. Rev. Sci. Eng. 33 (1991) 109.
[3] K. Fang, D. Li, M. Lin, M. Xiang, W. Wei, Y. Sun, Catal. Today 147 (2009) 133.
[4] V. Subramani, S.K. Gangwal, Energy Fuel 22 (2008) 814.
[5] G.J. Quarderer, G.A. Cochran, European Patent EP0119609, to The Dow Chemical Company, 1984.
[6] M.M. Conway, C.B. Murchison, R.R. Stevens, US Patent 4 675 344, to The Dow Chemical Company, 1987.
[7] G.J. Quarderer, G.A. Cochran, US Patent 4 749 724, to The Dow Chemical Company, 1988.
[8] R.R. Stevens, US Patent 4 752 622, to The Dow Chemical Company, 1988.
[9] R.R. Stevens, US Patent 4 882 360, to The Dow Chemical Company, 1989.
[10] R.B. Levy, M. Boudart, Science 181 (1973) 547.
[11] J.S. Lee, M. Boudart, Catal. Lett. 20 (1993) 97.
[12] J.S. Lee, S.T. Oyama, M. Boudart, J. Catal. 106 (1987) 125.
[13] J.S. Lee, S. Locatelli, S.T. Oyama, M. Boudart, J. Catal. 125 (1990) 157.
[14] J.G. Chen, Chem. Rev. 96 (1996) 1477.
[15] S.T. Oyama, Catal. Today 15 (1992) 179.
[16] K.Y. Park, W.K. Seo, J.S. Lee, Catal. Lett. 11 (1991) 349.
[17] H.C. Woo, K.Y. Park, Y.G. Kim, I. Nam, J.S. Chung, J.S. Lee, Appl. Catal. 75 (1991) 267.
[18] J.S. Lee, S. Kim, Y.G. Kim, Top. Catal. 2 (1995) 127.
[19] L. Leclercq, A. Almazouari, M. Dufour, in: The Chemistry of Transition Metal Carbides and Nitrides, Springer, 1996, p. 345.
[20] M. Xiang, D. Li, H. Xiao, J. Zhang, H. Qi, W. Li, B. Zhong, Y. Sun, Fuel 87 (2008) 599.
[21] M. Xiang, D. Li, H. Xiao, J. Zhang, W. Li, B. Zhong, Y. Sun, Catal. Today 131 (2008) 489.
[22] M. Xiang, D. Li, W. Li, B. Zhong, Y. Sun, Catal. Commun. 8 (2007) 88.
[23] M. Xiang, D. Li, W. Li, B. Zhong, Y. Sun, Catal. Commun. 8 (2007) 503.
[24] M. Xiang, D. Li, W. Li, B. Zhong, Y. Sun, Catal. Commun. 8 (2007) 513.
[25] N. Wang, K. Fang, M. Lin, D. Jiang, D. Li, Y. Sun, Catal. Lett. 136 (2010) 9.
[26] N. Wang, K. Fang, D. Jiang, D. Li, Y. Sun, Catal. Today 158 (2010) 241.
[27] L. Zhao, K. Fang, D. Jiang, D. Li, Y. Sun, Catal. Today 158 (2010) 490.
[28] J.T. Calla, R.J. Davis, J. Catal. 241 (2006) 407.

[29] R. Burch, M. Petch, Appl. Catal. A 88 (1992) 39.
[30] B. Fingland, F. Ribeiro, J. Miller, Catal. Lett. 131 (2009) 1.
[31] B. Ravel, M. Newville, J. Synchrotron Radiat. 12 (2005) 537.
[32] S. Zabinsky, J.J. Rehr, A. Ankudinov, R.C. Albers, M.J. Eller, Phys. Rev. B 52 (1995) 2995.
[33] W. Wu, Z. Wu, C. Liang, X. Chen, P. Ying, C. Li, J. Phys. Chem. B 107 (2003) 7088.
[34] M. Xiang, D. Li, W. Li, B. Zhong, Y. Sun, Fuel 85 (2006) 2662.
[35] H. Kim, K.H. Lee, J.S. Lee, Res. Chem. Intermed. 26 (2000) 427.
[36] V. Ponec, Catal. Today 12 (1992) 227.
[37] G. van der Lee, V. Ponec, Catal. Rev. Sci. Eng. 29 (1987) 183.
[38] A. Muramatsu, T. Tatsumi, H. Tominaga, Bull. Chem. Soc. Jpn. 60 (1987) 3157.
[39] J. Christensen, P. Mortensen, R. Trane, P. Jensen, A. Jensen, Appl. Catal. A 366 (2009) 29.
[40] A. Griboval-Constant, J. Giraudon, G. Leclercq, L. Leclercq, Appl. Catal. A 260 (2004) 35.
[41] G.S. Ranhotra, A.T. Bell, J.A. Reimer, J. Catal. 108 (1987) 40.
[42] A. Jentys, Phys. Chem. Chem. Phys. 1 (1999) 4059.
[43] S. Liu, L. Wang, R. Ohnishi, M. Ichikawa, J. Catal. 181 (1999) 175.
[44] W. Ding, S. Li, G. D Meitzner, E. Iglesia, J. Phys. Chem. B 105 (2001) 506.
[45] H.H. Hwu, M.B. Zellner, J.G. Chen, J. Catal. 229 (2005) 30.
[46] A. Sarkar, G. Jacobs, Y. Ji, H.H. Hamdeh, B.H. Davis, Catal. Lett. 121 (2008) 1.
[47] B.C. McClaine, S.E. Siporin, R.J. Davis, J. Phys. Chem. B 105 (2001) 7525.